

Separation of Scattering Mechanisms Through Multiple-Input Multiple-Output Synthetic Aperture Radar Tomography

Olena Sarabakha, Tobias Rommel, Gerhard Krieger, and Michelangelo Villano
Microwaves and Radar Institute
German Aerospace Center (DLR)
Weßling, Germany
olena.sarabakha@dlr.de

Abstract—Synthetic aperture radar (SAR) tomography is gaining increasing interest for its capability to reconstruct the vertical profile of natural and urban scenes. However, since large tomographic apertures will be used in the future in order to increase the vertical resolution of the three-dimensional reconstruction, an analysis of the far-field approximation is necessary to assess its validity in SAR tomography. In addition, it is of great importance to understand how different scattering mechanisms behave based on the selected tomographic SAR acquisition configuration. Multiple-input multiple-output (MIMO) SAR tomography has been proven to be able to detect and separate the contribution of single- and double-bounce scattering, allowing a more precise vertical reconstruction of the scene, and this capability will be assessed in an experiment with a MIMO measurement setup.

Keywords—Synthetic aperture radar (SAR), multiple-input multiple-output (MIMO), tomography, far-field, near-field, single-bounce, double-bounce, vector network analyzer (VNA).

I. INTRODUCTION

Synthetic aperture radar (SAR) has been widely used in the past decades in remote sensing imaging to create two-dimensional representations of the scene of interest [1-3]. Conventional SAR images are limited though by the fact that all the radar echoes returning from a circular ring centered at the platform position are focused in the same range-azimuth pixel, mixing the returns from different scatterers distributed in the elevation direction and preventing the possibility to reconstruct the third dimension of the scene. This limitation can be overcome using multiple SAR acquisitions at different cross-range (or elevation) positions, thus observing the scene from slightly different angles and allowing the reconstruction of the vertical structure of the scene [4-6]. However, this solution comes with some challenges. First, the tomographic apertures in elevation required for high vertical resolution are usually very large, in the order of kilometers for spaceborne SAR, yielding the necessity to analyze the validity of the far-field condition. Second, double-bounce scattering hinders the correct reconstruction of the vertical profile, due to incorrect positioning of the targets and masking of weaker scatterers due to its high backscattered power. As has already been assessed in [7], double-bounce scattering has different behaviors based on the configuration of the tomographic acquisition. A tomogram can be acquired mainly in three ways: monostatic repeat-pass, namely one satellite flying several times over the same region and acquiring a time-series of images; multistatic single-pass, with several receiving and one transmitting satellite flying in formation and acquiring several bistatic images in the same moment; multiple-input multiple-output (MIMO) single-pass, where a few satellites fly in formation and transmit and receive at the same time, acquiring several monostatic and bistatic images of the scene. In particular, MIMO systems have gained increasing interest

in the past years, as they offer a significant improvement in imaging performance, at the cost of some technical complications [8-10]. A few solutions for double-bounce scattering suppression using MIMO systems have already been proposed in [11], using digital beamforming on both receive and transmit, and in [12], exploiting a variation of the compressive sensing (CS) algorithm in order to separate single- and double-bounce scattering.

II. NEAR-FIELD VS FAR-FIELD ANALYSIS

In the far-field approximation it is assumed that the electromagnetic wave received by the different elements of the antenna array is a planar wave (planar wavefront model), as in Fig. 1. This allows correcting for the phase shift between the antenna elements and obtaining the focused signal, s_f :

$$s_f = \sum_{n=1}^N s_n \cdot \exp\left(+j2m\frac{\pi}{\lambda}nb_{el}\sin\theta\right) \quad (1)$$

where s_n , $n = 1, \dots, N$ are the raw signals, $m = 1$ and $m = 2$ for multistatic and monostatic acquisitions, respectively, λ is the wavelength, b_{el} is the distance between two consecutive antenna elements, θ is the direction of arrival of the signal, and N is the total number of receivers. This approximation is valid when the target that is producing the radar echo is in the far-field condition, i.e., according to the Fraunhofer formulation when:

$$R_0 \gg \frac{2L^2}{\lambda} \quad (2)$$

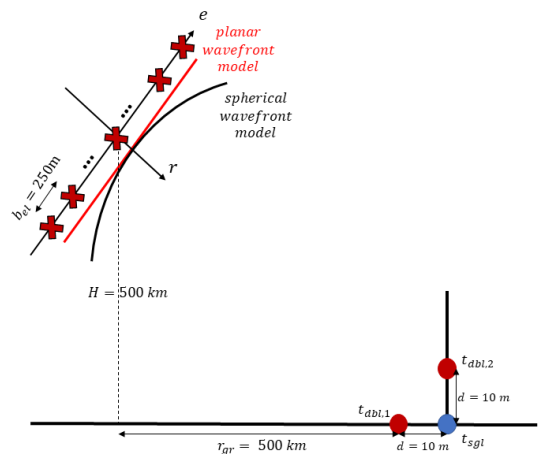


Fig. 1. Simulation geometry. The red crosses represent the equivalent phase centers for the three considered acquisition modes. The red straight line represents the planar wavefront model, the black line represents the spherical wavefront model on the tomographic aperture.

where R_0 is the slant range of the target and L is the length (or aperture) of the antenna array. When considering apertures in the order of kilometers, the far-field condition is hardly satisfied for typical orbital heights (and ranges) of SAR systems and the target usually lies in the near-field. As a consequence, the far-field approximation causes an incorrect focusing of the signal, with consequent loss of gain and deformation of the point spread function (PSF). In order to avoid such effects, the signal must be processed using the near-field geometry, correcting the phase shifts on the antenna elements using the actual distances between the SAR satellites and the target, assuming that the received wave front is spherical (spherical wavefront model), as in (3):

$$s_f = \sum_{n=1}^N s_n \cdot \exp\left(+2j\frac{\pi}{\lambda} (\|r_{tx} - r_{tg}\| + \|r_{rx} - r_{tg}\|)\right) \quad (3)$$

where $\|\cdot\|$ is the Euclidean norm, r_{tx} and r_{rx} are the positions of transmit and receive antennas, respectively (notice that they coincide in case of monostatic acquisitions), and r_{tg} is the target position.

To demonstrate the inadequacy of the far-field approximation in the case of a kilometer-long tomographic aperture, three simulations using the parameters in Table I have been carried out considering a point-like target and only single-bounce scattering. The Rayleigh resolution [13] for such system is:

$$\delta_{el} = \frac{\lambda}{\alpha L} R_0 \quad (4)$$

where $\alpha = 2$ for monostatic acquisition, $\alpha = 1$ for multistatic acquisitions, and $1 \leq \alpha \leq 2$ for MIMO mode [14]. As the spacing between the antenna elements is much greater than $\lambda/2$, grating lobes are expected to appear on the elevation axis:

$$A = \pm k \frac{\lambda}{mb_{el}} R_0 \quad (5)$$

where m is the same coefficient as in (1), and k is an integer other than 0. Notice that the satellites are distributed in such a way to obtain the same phase centers, namely the tomographic baseline in the multistatic and MIMO cases is double with respect to the monostatic baseline. In this way, the Rayleigh resolution and the ambiguities are similar for the three systems, making the comparison between PSFs easier. For the analysis presented in this abstract, the processing consists of beamforming in elevation and, in the MIMO case, all channels are summed coherently. As shown in Fig. 2, the near-field processing yields the same results for all the

considered tomographic modes, with the expected values for resolution and ambiguity positions. On the other hand, when the signal is processed with the far-field approximation, the PSF is completely deformed in all three cases, with a significant loss in gain.

In order to have a systematic analysis on the validity of the far-field approximation in spaceborne SAR tomography, in Fig. 3 is shown the maximum tomographic aperture that can be used in order to be in the far-field condition, considering typical wavelengths and slant ranges for SAR systems. It must be underlined though that the far-field approximation may still work for slightly larger tomographic apertures than those indicated in Fig. 3, with an acceptable gain loss and deformation of the target response, and this aspect should be further investigated.

TABLE I. SYSTEM PARAMETERS

System parameter	Symbol	Value
Number of satellites	N	10
Tomographic baseline	b_{el}	250 m (monostatic) 500 m (multistatic, MIMO)
Tomographic aperture	L	2500 m (monostatic) 5000 m (multistatic, MIMO)
Central frequency	f_0	9.65 GHz
Incidence angle	θ_i	45°
Rayleigh resolution	δ_{el}	~3.88 m
First ambiguity	A_1	±44 m

III. SCATTERING MECHANISMS IN MONOSTATIC AND MULTISTATIC ACQUISITIONS

In this section the different behavior of the double-bounce scattering mechanism in different tomographic modes will be analyzed. The simulation geometry is the same as in Fig. 1. Two point-like targets are used to simulate the double-bounce scattering in monostatic repeat-pass, multistatic single-pass, and MIMO single-pass acquisitions. The acquisition parameters are the same as in Table I. As shown in Fig. 4, the double-bounce response in the monostatic case is equivalent to the single-bounce response, with only one target focused at elevation zero. This is due to the fact that in the monostatic case the double-bounce path length corresponds to the single-bounce path length and therefore the same elevation response. On the other hand, both in the multistatic and MIMO cases two targets appear at around the actual elevation of the two double-bounce scatterers. This effect is due to an antenna-target range variation across the tomographic aperture which

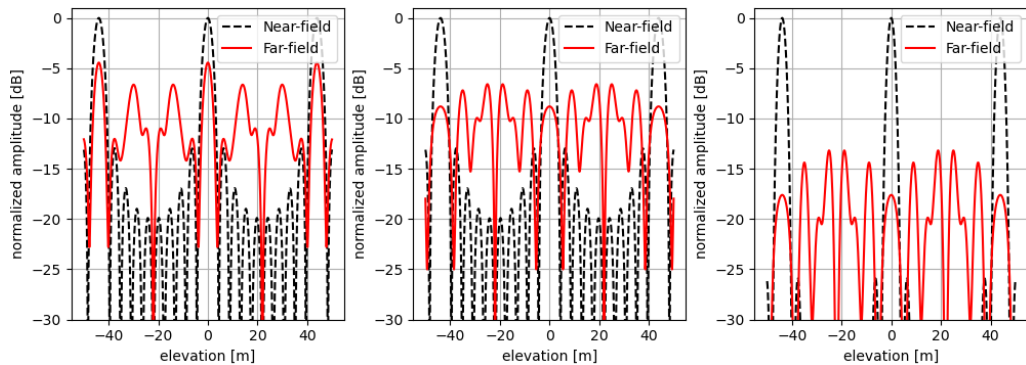


Fig. 2. Comparison of single-bounce scattering using near-field (dashed black) and far-field (solid red) processing for: left, monostatic; center, multistatic; right, MIMO.

causes, after focusing, a linear residual phase with a slope proportional to the elevation position of the target and to the distance between the transmit and receive antennas. This residual phase corresponds to a beam steering towards the actual position of the last target that has reflected the signal. As in the MIMO mode, both monostatic and multistatic acquisitions are mixed together, the resulting response in elevation does not show a single peak for each target, but rather a group of peaks. This different behavior of the double-bounce scattering in multistatic acquisitions can be exploited to detect and suppress this scattering mechanism and obtain a SAR tomogram with only single-bounce scattering, leading to a more precise reconstruction of the vertical profile of the scene.

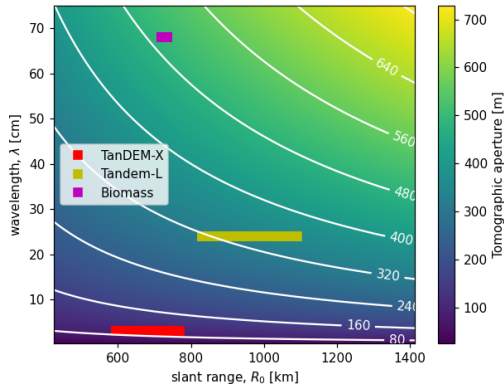


Fig. 3. Maximum tomographic aperture in order to satisfy the far-field condition for typical wavelengths and slant ranges for SAR systems. As an example, the horizontal bars show the results for: TanDEM-X (red), Tandem-L (yellow), and Biomass (magenta).

IV. EXPERIMENTAL DEMONSTRATION USING A VECTOR NETWORK ANALYZER

In order to demonstrate the capability of MIMO SAR tomography to separate single- and double-bounce scattering, an experiment with a MIMO demonstrator using a vector network analyzer (VNA) will be carried out. The system is composed by two separate antenna arrays for transmit and for receive with a small horizontal (azimuthal) separation in order to avoid coupling or interference. These antenna arrays will be mounted on a building rooftop, pointing at the scene of interest on the ground below. The scene will be composed of different targets, such as spheres and orthogonal metal plates to produce double-bounce scattering, and corner reflectors for calibration. The experiment can be carried out both in real aperture radar mode (ignoring the azimuthal direction for simplicity) and SAR mode by taking acquisitions while

moving the two arrays along the azimuth direction. Since the observed scene is assumed to be stationary, time multiplexing for the signal will be used to synthesize the MIMO acquisition. This solution is necessary to limit additional errors introduced by complex orthogonal waveforms, which are required to have a full MIMO acquisition. In addition, the experiment will be carried out in both horizontal and vertical polarizations in order to analyze any difference in the tomographic response with respect to the polarimetric mode. This experiment will allow comparing the performance of the digital beamforming on receive and on transmit and the CS-based single- and double-bounce scattering separation.

V. CONCLUSIONS

In this abstract, the differences between the far-field and near-field processing in SAR tomography have been discussed. In particular, the far-field approximation has been proven to be inadequate for acquisitions that use tomographic apertures in the order of kilometers. As a consequence, the near-field processing should be used in order to avoid gain loss and deformation of the response of the observed scene. In addition, the different behavior of double-bounce scattering based on the tomographic acquisition mode has been shown. In particular, single- and double-bounce scattering cannot be distinguished in monostatic repeat-pass tomography, leading to erroneous vertical profile reconstructions. In multistatic single-pass tomography, single-bounce and double-bounce scattering lead to different responses, but the reconstructed vertical profile could still be misleading, as double-bounce scatterers could be erroneously positioned below ground level or mask the single-bounce response of weaker scatterers. The proposed solution is to use MIMO SAR tomography with multiple transmitters and multiple receivers, which will allow to correctly reconstruct the vertical profile of the scene by separating single- and double-bounce scattering. This will allow also to retrieve some additional information about the structure of the scene, as double-bounce scattering is usually produced by two orthogonal surfaces. The results of the MIMO-demonstrator experiment will be presented in the final paper.

ACKNOWLEDGMENT

This work was partially funded by the European Union (ERC, DRITUCS, 101076275). Views and opinions expressed are however those of the authors only and do not necessarily reflect those of the European Union or the European Research Council Executive Agency. Neither the European Union nor the granting authority can be held responsible for them.

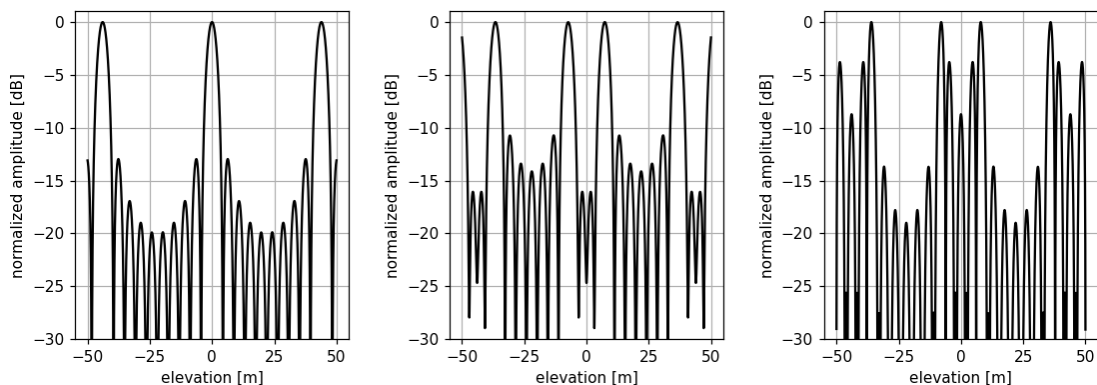


Fig. 4. Elevation response of double-bounce scattering for: left, monostatic; center, multistatic; right, MIMO.

REFERENCES

- [1] A. Moreira, P. Prats-Iraola, M. Younis, G. Krieger, I. Hajnsek and K. P. Papathanassiou, "A tutorial on synthetic aperture radar", in *IEEE Geoscience and Remote Sensing Magazine*, vol. 1, no. 1, pp. 6-43, March 2013.
- [2] C. Elachi, *Spaceborne Radar Remote Sensing: Applications and Techniques*. New York, NY, USA: IEEE Press, 1988.
- [3] F. M. Henderson and A. J. Lewis, Eds., *Manual of Remote Sensing: Principles and Applications*. New York, NY, USA: Wiley, 1998.
- [4] A. Reigber, A. Moreira and K. P. Papathanassiou, "First demonstration of airborne SAR tomography using multibaseline L-band data", *IEEE 1999 International Geoscience and Remote Sensing Symposium. IGARSS'99 (Cat. No.99CH36293)*, Hamburg, Germany, 1999, pp. 44-46 vol.1.
- [5] G. Fornaro, V. Pascazio, "SAR Interferometry and Tomography: Theory and Applications", *Academic Press Library in Signal Processing*, Volume 2, 2014, Pages 1043-111.
- [6] H. Aghababaei et al., "Forest SAR Tomography: Principles and Applications", in *IEEE Geoscience and Remote Sensing Magazine*, vol. 8, no. 2, pp. 30-45, June 2020.
- [7] G. Krieger, T. Rommel and A. Moreira, "MIMO-SAR Tomography", *EUSAR*, June 2016.
- [8] G. Krieger, "MIMO-SAR: Opportunities and Pitfalls", in *IEEE Transactions on Geoscience and Remote Sensing*, vol. 52, no. 5, pp. 2628-2645, May 2014.
- [9] G. Krieger et al., "MIMO-SAR and the orthogonality confusion", *2012 IEEE International Geoscience and Remote Sensing Symposium*, Munich, Germany, 2012, pp. 1533-1536.
- [10] G. Krieger et al., "Digital beamforming and MIMO SAR: Review and new concepts", *EUSAR 2012; 9th European Conference on Synthetic Aperture Radar*, Nuremberg, Germany, 2012, pp. 11-14.
- [11] T. Rommel and G. Krieger, "Detection of Multipath Propagation Effects in SAR-Tomography with MIMO Modes", *Proceedings of EUSAR 2016: 11th European Conference on Synthetic Aperture Radar*, Hamburg, Germany, 2016, pp. 1-5.
- [12] F. Zhang, X. Liang, R. Cheng, Y. Wan, L. Chen and Y. Wu, "Building Corner Reflection in MIMO SAR Tomography and Compressive Sensing-Based Corner Reflection Suppression", in *IEEE Geoscience and Remote Sensing Letters*, vol. 17, no. 3, pp. 446-450, March 2020.
- [13] Richards, M.A.; Scheer, J.A.; Holm, W.A. (Eds.) *Principles of Modern Radar: Basic Principles*; Institution of Engineering and Technology: Stevenage, UK, 2010.
- [14] I. Seker, M. Lavalle, "Tomographic Performance of Multi-Static Radar Formations: Theory and Simulations", *Remote Sens.* 2021, 13(4), 737.